


Metal-semiconductor transition in the supercooled liquid phase of the $\text{Ge}_2\text{Sb}_2\text{Te}_5$ and GeTe compounds

M. Cobelli , D. Dragoni,^{*} S. Caravati, and M. Bernasconi 

Dipartimento di Scienza dei Materiali, Università di Milano-Bicocca, Via R. Cozzi 55, I-20125, Milano, Italy



(Received 30 November 2020; accepted 10 March 2021; published 20 April 2021)

The $\text{Ge}_2\text{Sb}_2\text{Te}_5$ and GeTe compounds are of interest for applications in phase change memories. In the reset process of the memory the crystal is rapidly brought above the melting temperature T_m by Joule heating and then the liquid phase rapidly cools down leading to the formation of the amorphous phase. Since the liquid above T_m is metallic and the amorphous phase is semiconducting a semiconductor-to-metal transition occurs in the supercooled liquid. Based on density functional simulations, we estimated the metal-semiconductor transition temperature $T_{\text{M-SC}}$ by monitoring the opening of a band gap in the supercooled liquid phase. Due to previous evidence on the importance of the van der Waals (vdW) interaction in describing the liquid phase of these materials, we used both the revised Vydrov-van Voorhis functional which includes vdW nonlocal interactions and the Perdew-Burke-Ernzerhof functional without vdW corrections. The estimated $T_{\text{M-SC}}$ is about 100–150 K higher with the former than with the latter framework for both compounds. By including vdW interactions the estimated $T_{\text{M-SC}}$ is closer to T_m than to the glass transition temperature for both systems. The analysis of the structural properties as a function of temperature suggests a correlation between the metal-semiconductor transition and a Peierls distortion. However, the data support more a continuous structural transformation than the presence of a first order liquid-liquid phase change associated the metal-semiconductor transition.

DOI: [10.1103/PhysRevMaterials.5.045004](https://doi.org/10.1103/PhysRevMaterials.5.045004)

I. INTRODUCTION

Phase change memories (PCMs) are one of the leading candidates for the realization of storage-class memories which combine nonvolatility with speed and endurance close to those of the dynamic random access memories (DRAM) [1]. PCMs exploit a fast and reversible transformation between the crystalline and amorphous phases of chalcogenide alloys due to Joule heating. The material of choice for PCMs is presently the ternary compound $\text{Ge}_2\text{Sb}_2\text{Te}_5$ (GST) [2–4], although doping of the parent binary compound GeTe and Ge-rich GeSbTe alloys are also exploited for applications that require operation at high temperatures [5,6]. These materials are degenerate p-type semiconductors in the crystalline phase with a high electrical conductivity while they behave as intrinsic semiconductors in the amorphous phase with a lower conductivity and a Fermi level pinned at or close to midgap [2,7]. The state of the memory is read by the measurement of the resistance that differs by about three orders of magnitude between the two phases.

In the reset process of the memory, the crystal is rapidly brought above the melting temperature T_m by an intense and short current pulse. Then, the liquid rapidly cools down below T_m turning into the amorphous phase at the glass transition temperature T_g . Electronic structure calculations based on Density Functional Theory (DFT) revealed that liquid $\text{Ge}_2\text{Sb}_2\text{Te}_5$ and GeTe, as well as many others phase change materials, show a pseudogap in the electronic density of states

(DOS) close to the Fermi level E_F which is progressively filled by increasing temperatures [8–13]. Since the experimental electronic conductivity increases with temperature [14–16] these materials are often referred to as semiconductor liquids, although the raise in conductivity above T_m might not be due to a higher density of thermally excited carriers but to an increase of the density of delocalized states at E_F . Nevertheless, the conductivity is often fitted with an Arrhenius form with a temperature dependent apparent activation energy. The temperature at which the activation energy reaches a maximum is often defined operatively as the metal-semiconductor transition temperature [17]. However, a suitable definition of the metal-semiconductor transition (M-SC) is given by the temperature $T_{\text{M-SC}}$ at which a mobility gap opens up by decreasing temperature. This is the definition of $T_{\text{M-SC}}$ we use hereafter.

The experimental measurement of $T_{\text{M-SC}}$ in phase change materials, would it occur below T_m , is hampered by their extremely fast crystallization. This feature is believed to originate from the high fragility of the supercooled liquid phase whose viscosity remains fairly low below T_m , only to rise sharply in a non-Arrhenius manner very close to T_g [18–20]. On the contrary, in a strong liquid the viscosity follows an Arrhenius behavior with a single activation energy from T_m and T_g . The fragility actually boosts the crystallization speeds because it allows for a high atomic mobility at high supercooling where the thermodynamical driving force for crystal nucleation and growth is also large [18]. In this context, a precise location of the M-SC transition is also of interest because it has been suggested that $T_{\text{M-SC}}$ might control a strong-to-fragile crossover in the temperature dependence of the viscosity [21].

^{*}daniele.dragoni@unimib.it

In turn, a strong-to-fragile transition sufficiently close to T_g would guarantee a fast crystallization for the reasons outlined above and at the same time a higher stability of the amorphous phase whose aging propensity is usually larger the higher is the fragility close to T_g [22,23].

Previous DFT molecular dynamics (MD) simulations of $\text{Ge}_2\text{Sb}_2\text{Te}_5$ [8] and GeTe [9] have shown a deepening of the pseudogap at E_F upon cooling from temperatures slightly above to slightly below T_m . This has been ascribed to an enhancement of the Peierls distortion consisting of the formation of long and short bond around Ge and Sb atoms [8,9]. These simulations were, however, restricted to temperatures where the DOS at E_F and the resulting electrical conductivity is still relatively high.

In this work, we extend the previous DFT investigations by analyzing the electronic properties of $\text{Ge}_2\text{Sb}_2\text{Te}_5$ and GeTe at high supercooling below T_m down to temperatures close to T_g aiming at identifying the appearance of a mobility gap and thus at estimating T_{M-SC} . We mention that a combined DFT and experimental study of the metal-semiconductor transition was recently reported also for the supercooled phase of the $\text{Ge}_{15}\text{Sb}_{85}$ phase change alloy [24].

II. COMPUTATIONAL DETAILS

We performed Born-Oppenheimer DFT molecular dynamics simulations by using the CP2k suite of programs [25,26]. Goedecker-type pseudopotentials with four, three and six valence electrons were used for Ge, Sb, and Te [27]. The Kohn-Sham (KS) orbitals were expanded in the basis set of triple-zeta-valence plus polarization (TZVP) Gaussian-type orbitals (GTO) while the charge density was expanded in a plane-wave basis set with a cut-off of 100 Ry to efficiently solve the Poisson equation within the Quickstep scheme [25,26]. Brillouin Zone (BZ) integration was restricted to the supercell Γ point. The same scheme was applied in our previous work on several other phase change compounds [28–33].

There is evidence in literature that the inclusion of van der Waals (vdW) interactions is important to properly describe the structural properties of the liquid above T_m of GeTe and $\text{Ge}_2\text{Sb}_2\text{Te}_5$ [8,9]. Therefore, we used the exchange and correlation functional including vdW interaction proposed by Vydrov and van Voorhis [34] and revised by Sabatini *et al.* (rVV10) [35]. For this functional the gradient corrected Perdew-Burke-Ernzerhof (PBE) functional is used for the semilocal correlation energy [36]. We thus used PBE norm conserving pseudopotentials as it is commonly reported in literature, although they are not fully consistent with the rVV10 functional. For the sake of comparison we also repeated all the simulations with the mostly used PBE functional with no vdW corrections to see their effect on the estimated T_{M-SC} .

MD simulations in supercell with periodic boundary conditions were performed by using the predictor-corrector scheme of Refs. [37,38] for the self-consistent solution of KS equation at each MD step, 2 fs long.

Liquid GST was modeled in an orthorhombic supercell containing 270 atoms with edges of 21.971 Å, 21.971 Å, and 18.643 Å corresponding to a density of 5.683 g/cm³ (0.0300 atoms/Å³), which is close to the experimental value in the temperature range of interest [8]. Liquid GeTe was

modeled by a 216-atom cubic supercell with a cell edge of 18.643 Å corresponding to a density of 5.542 g/cm³ (0.0333 atoms/Å³), which is close to the experimental one of the amorphous phase [5]. The volume was held fixed during the quenching protocol as it changes very little between the liquid at T_m and the amorphous phase at T_g . For instance, the experimental density of liquid [39] GeTe at T_m is 0.0339 atom/Å³, while the density of the amorphous phase [5] is 0.0332 atom/Å³. The liquid models were generated by first thermalizing the system slightly above the experimental T_m (998 K for GeTe, [39] 858–877 K for GST [16,40]).

We quenched the GST (GeTe) models from 1000 K (900 K) in steps of 100 K by equilibrating the system for 15 ps before reducing the temperature. We also considered intermediate temperatures to better locate T_{M-SC} by reducing the temperature by 50 K from the nearest higher temperature of the quenching protocol. These branched-off configurations have been used as a starting point for new MD simulations consisting of 2.3 ps of equilibration plus a canonical run 15 ps long. The quenching rate of our protocol of 6.6 K/ps (100 K/15 ps) is similar to those used to generate the amorphous models in several previous works where the overall quenching time from 1000 K to 300 K was about 100 ps [41,42].

We have not investigated the dependence of the electronic DOS on the quenching rate. However, a previous analysis on $\text{Ge}_2\text{Sb}_2\text{Te}_5$ shows minor changes in the structural properties of the amorphous phase by doubling the quenching rate from 5 to 10 K/ps [43]. Reducing the quenching rate to 1 K/ps lead instead to partial crystallization as this material is a very poor glass former [43]. In another work [44], it was shown that two amorphous models of GeTe generated by quenching from 1000 K to 300 K in either 100 ps or 3 ns featured very similar structural properties provided that in the long quench (3 ns) the quenching rate was faster (≥ 1 K/ps) in the 700–500 K range to prevent crystallization. Several simulations of the supercooled liquid phases of GeTe and $\text{Ge}_2\text{Sb}_2\text{Te}_5$ show that the time scale of few tens of ps used in our production runs is much shorter than the typical incubation time (several hundreds of ps) for the formation of crystalline nuclei in the temperature range 700–500 K where nucleation rate and crystal growth velocities are high [44–46]. Average temperatures were computed over about 15 ps of production canonical runs with a Langevin thermostat [38].

The electronic density of states (DOS) were computed by averaging over nine snapshots of the rVV10 trajectories at different temperatures in the supercooled liquid phase in the range 900–500 K. For each snapshot the KS orbitals were computed at the supercell Γ -point with the HSE06 hybrid functional [47] to better reproduce the band gap as already done in our previous study of the crystalline phase [28]. KS energies were broadened by a Gaussian function with a variance of 27 meV. The DOS of the different snapshots at the same temperature are aligned at the highest occupied state for the sake of a clear visual representation of the opening of the band gap. The highest occupied state is obtained in turn by integrating the DOS under the constraint on the total number of electrons. Different alignments of the DOS were also checked by using the bottom of p bands or the bottom of the band of Te 5s states shown in Fig. S1 in the

Supplemental Material (SM) [48]. In both cases the change in the DOS is within the standard deviation over the nine snapshots. The Fermi level E_F is then assigned by $n = \int D(\epsilon) f_{FD}(\epsilon) d\epsilon$ where $D(\epsilon)$ is the DOS averaged over the nine snapshots, n is the electron density and f_{FD} is the Fermi-Dirac distribution at the corresponding temperature. At all temperatures the Fermi level is then set to the zero of energy.

To quantify the localization properties of individual KS states, we have computed the inverse participation ratio (IPR), which is defined for the i th KS state by $\sum_j c_{ij}^4 / (\sum_j c_{ij}^2)^2$, where j runs over the GTOs of the basis set and c_{ij} are the expansion coefficients of the i th KS state in GTOs. The IPR takes values varying from $1/N$ for a completely delocalized electron, where N is the number of atomic-like orbitals in the basis set of the whole supercell, to one for an electron completely localized on a single atomic-like orbital.

We also computed the imaginary part of the dielectric function $\varepsilon_2(E)$ to estimate the Tauc gap as it will be defined later. In the random phase approximation, $\varepsilon_2(E)$ is given by

$$\varepsilon_2(E) = \frac{8\pi^2 e^2 \hbar^2}{3m^2 V_o N_{\mathbf{k}} E^2} \sum_{v,c,\mathbf{k}} |\langle c, \mathbf{k} | \mathbf{p} | v, \mathbf{k} \rangle|^2 \delta(E - E_{c,\mathbf{k}} + E_{v,\mathbf{k}}), \quad (1)$$

where $E_{c,\mathbf{k}}$ and $E_{v,\mathbf{k}}$ refer to the KS energies of conduction (empty) and valence (filled) bands at the $N_{\mathbf{k}}$ \mathbf{k} -points in the supercell BZ, m and e are the mass and charge of the electron. We restricted the calculation to the Γ -point of the supercell with volume V_o . In the actual calculation the δ -functions are substituted by Gaussian functions with variance of 27 meV. Neglecting local field effects has been proven to be adequate in previous calculations on other phase change tellurides [49,50]. The same approach was employed in our previous study of the optical properties of amorphous and crystalline GeTe, GST, and Sb_2Te_3 [50].

III. RESULTS

The identification of the mobility gap from DFT simulations is a challenging task due to limitation in size of the supercells that can be used and the consequent difficulties in performing a finite size scaling analysis to assess the localization length of the electronic states. Thus, we tried to estimate the opening of a mobility gap in an approximate manner as described below. It has been shown that the electronic DOS as a function of energy $D(E)$ close to the band gap of models of amorphous GST and GeTe can be reliably described by square-root functions as $\sqrt{E - E_c}$ and $\sqrt{E_v - E}$ where E_c and E_v are the conduction and valence band edges supplemented by Urbach tails and eventually deep localized states in the energy gap ($E_g = E_c - E_v$) [51,52]. By heating the amorphous phase above T_g one expects that the energy gap E_g defined above would decrease and that at the same time the density of localized states in the gap would increase as well. At a given temperature we expect E_g to vanish which would represent a lower bound to T_{M-SC} (metal-semiconductor transition) if the finite density of states at E_F still refers to localized states. On the contrary, a finite band gap as defined above might also coexist with a finite density of delocalized states at E_F . Therefore, from the analysis of the DOS we estimate the temperature at which E_g vanishes and from visual inspection

of the IPR we assess whether the states at E_F are localized or not.

As a different estimate of the gap closure, we computed the optical Tauc gap from the imaginary part of the dielectric function $\varepsilon_2(E)$. The optical Tauc gap is defined as the energy E for which the linear extrapolation of the function $E\sqrt{\varepsilon_2(E)}$ becomes zero (Tauc plot).

In the following we report the results on the DOS, IPR and the estimate of the electronic gap by the two methods described above for liquid $\text{Ge}_2\text{Sb}_2\text{Te}_5$ and GeTe below and just above the experimental T_m in two separate subsections. We remark that the values of T_m and T_g we refer to in the text are always experimental values. We assign T_{M-SC} in the temperature range where the energy gap defined in two different manner vanishes with no strongly localized states at E_F . All the data reported in the following refer to the rVV10 simulations, if not otherwise specified, the corresponding data for the PBE simulations are given in the SM [48].

A. $\text{Ge}_2\text{Sb}_2\text{Te}_5$

The DOS close to E_F is reported in Fig. 1 for six different temperatures. At high temperature, close to the experimental T_m (858-877 K) [16,40], the system is clearly metallic with a high value of the DOS at E_F . Still, the DOS has a minimum at E_F which becomes more pronounced upon cooling. The pseudogap is somehow deeper than in previous DFT calculations [8] with a different vdW functional (DFT-D2) [53] at temperatures close and above T_m . Upon cooling the Fermi level shifts to lower energies with respect to the minimum of the DOS. The DOS close to the pseudogap below and above E_F have been fitted by functions of the type $A_v\sqrt{E_v - E}$ and $A_c\sqrt{E - E_c}$ as shown in Fig. 1, with A_v , E_v , A_c , and E_c as fitting parameters reported in Table SI in SM [48].

The band edges E_c and E_v obtained from the fitting provide an estimate of the band gap $E_g = E_c - E_v$. The resulting E_g as a function of temperature collected in Fig. 2 suggests a vanishing electronic gap at about 850 K.

However, a negative value of E_g might not necessarily imply a metallic behavior as the finite DOS at E_F might be due to localized states. Conversely, a positive E_g does not imply a semiconducting behavior if a finite density of delocalized states is still found at E_F . To assess the localization properties of the electronic states we superimpose the IPR to the DOS in Fig. 3. A sizably large IPR for the states in the pseudogap are found only at and below 796 K which is consistent with the estimate of T_{M-SC} at around 850 K (the nearest higher temperature considered here) given by the vanishing of E_g .

The DOS and the IPR over a wider energy range are reported in Fig. S1 in the SM [48] for the six different temperatures. The DOS and the IPR for the PBE simulations are given in Figs. S2–S4 in the SM [48]. The E_g as a function of temperature for the PBE simulations are compared in Fig. 2 with the rVV10 results. For both simulations the electronic DOS has been then computed with the hybrid HSE06 functional. The M-SC transition in the PBE simulations occurs at around 700 K, which is below the value of about 850 K for T_{M-SC} estimated from the rVV10 simulations. We will comment on this difference later on. First, we report on the analysis of the Tauc plot as a second manner to estimate the opening of the mobility gap.

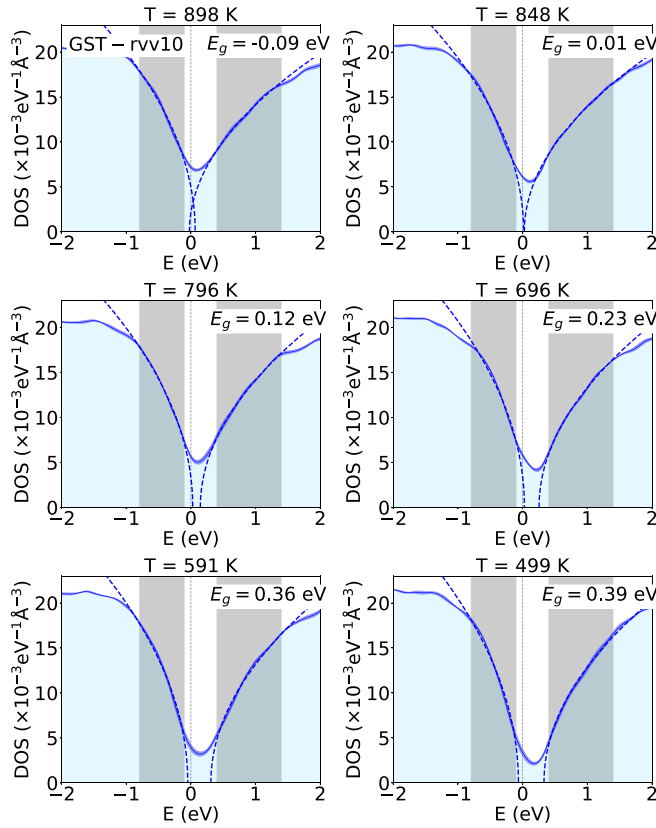


FIG. 1. Electronic density of states (DOS) around the Fermi level of the liquid and supercooled liquid $\text{Ge}_2\text{Sb}_2\text{Te}_5$ models generated with the rVV10 functional at different temperatures. The DOS are obtained from Kohn-Sham energies computed with the HSE06 functional and broadened with Gaussian functions 27 meV wide. The DOS is averaged over nine configurations at each temperature, the DOS of the different configurations are aligned at the highest occupied state. Standard deviations are depicted by the blue shaded area around the solid lines. Different alignments of the DOS were also checked (see Sec. II). In all cases the change in the DOS is within the standard deviation over the nine snapshots. The zero of energy is the Fermi level assigned by the average DOS at each temperature and the constraint on the total number of electrons. The fitting of the conduction and valence band edges with the square-root functions $A_c\sqrt{E-E_c}$ and $A_v\sqrt{E_v-E}$ in the gray shaded regions are also shown (dashed lines). The fitting parameters A_v , E_v , A_c and E_c are given in Table SI in SM [48]. The resulting band gap $E_g = E_c - E_v$ is given in each panel.

The Tauc plots at different temperatures are shown in Fig. 4 for the rVV10 functional, the corresponding plot for the PBE functional is reported in Fig. S5 in the SM [48]. The resulting Tauc gaps reported in Fig. 2 vanishes at a temperature remarkably close to that at which the E_g extracted from the DOS closes. This result gives us further confidence on our estimate of $T_{\text{M-SC}}$.

In our previous work on In_2Te_5 , we have associated the opening of a mobility gap in the supercooled liquid with a structural transformation consisting of the disappearance of defective octahedral configurations (bonding angles at about 90° and 180° but coordination lower than six) around In atoms [13]. Indeed, In atoms are mostly in tetrahedral coordination

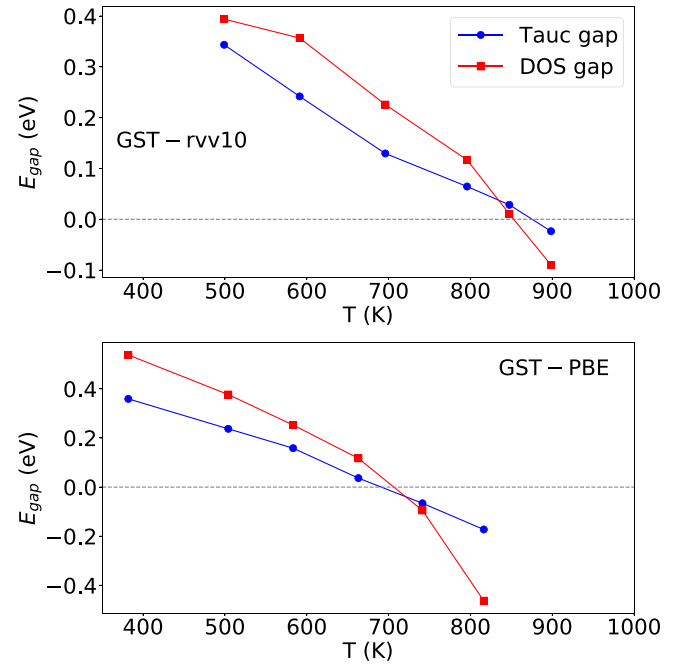


FIG. 2. (Upper panel) Energy gap as a function of temperature in the rVV10 simulations of GST obtained from the fitting of the electronic DOS close to E_F (red squares) shown in Fig. 1 or given by the Tauc optical gap (blue circles) computed from the plots in Fig. 4 (see text). The lines are just a guide for the eye. (Lower panel) The same of the upper panel for PBE simulations of GST.

and the minority of defective octahedral configurations contribute to the DOS at E_F [13]. In the case of $\text{Ge}_2\text{Sb}_2\text{Te}_5$ and GeTe , defective octahedra are the majority of configurations for Ge and Sb atoms. Tetrahedral configurations for Ge do appear upon cooling and correspond to about 30% of Ge atoms in DFT models of the amorphous phase of $\text{Ge}_2\text{Sb}_2\text{Te}_5$ [30] and GeTe [29]. However, tetrahedra can be detected only at temperatures lower than our estimated $T_{\text{M-SC}}$ as shown in Fig. 5 reporting the order parameter for tetrahedrality q introduced in Ref. [54] and used for phase change materials for instance in Refs. [13,30]. The order parameter is defined by $q = 1 - \frac{3}{8} \sum_{i>k} (\frac{1}{3} + \cos \theta_{ijk})^2$, where the sum runs over the pairs of atoms bonded to a central atom j and forming a bonding angle θ_{ijk} , [54] it evaluates to $q = 1$ for the ideal tetrahedral geometry and to $q = 5/8$ for a 4-fold coordinated defective octahedral site. The peak in the q distribution corresponding to tetrahedra is visible only at about 500 K and below, which excludes any correlation between the gap closure and the disappearance of tetrahedra. Note that the tetrahedra are more abundant in the PBE simulations than in rVV10 ones at similar temperatures, while $T_{\text{M-SC}}$ is higher for rVV10 than for PBE which further support the conclusions that the SC-M transition is not driven by the disappearance of tetrahedra upon heating. Further information on the evolution of the structural properties with temperature is provided by the partial pair correlation functions reported in Fig. 6 and by the angle distribution functions and the distribution of coordination numbers at different temperatures reported in Figs. S6-S7 in the SM [48].

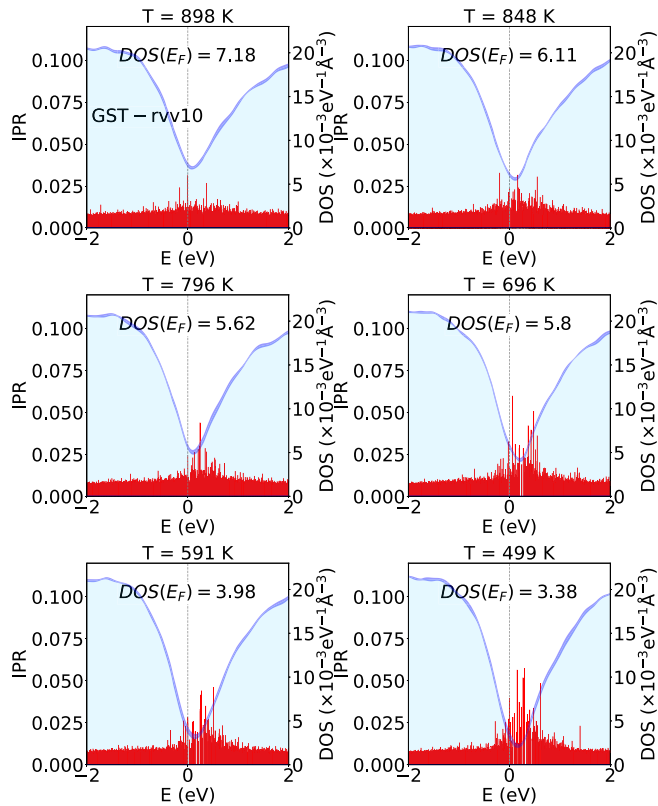


FIG. 3. Electronic density of states (DOS) around the Fermi level of the liquid and supercooled liquid GST models generated with the rVV10 functional at different temperatures as reported in Fig. 1 with the inverse participation ratio (IPR) superimposed to highlight the rising of localized states in the pseudogap as temperature is lowered. The IPR refers to the same nine configurations used to compute the DOS. The value of the DOS at the Fermi level is given in each panel.

The partial pair correlation functions show the presence of a larger fraction of Ge-Ge bonds at high temperatures in the PBE simulations than in the rVV10 ones. In a previous work, we have shown that the localized states in the gap of the semi-conducting amorphous phase of the parent compound GeTe are mostly due to the presence of chains of homopolar Ge-Ge bonds [55]. The Ge-Ge bonds are present in a larger amount in the liquid phase and they survive during the quenching to T_g . Homopolar bonds are not present in the crystalline phase and they are therefore often referred to as wrong bonds. We might therefore conceive that, analogously to GeTe, wrong bonds (Ge-Ge, Sb-Ge, Sb-Sb) could also be responsible for states at the Fermi level. The larger the amount of these states the lower is the T_{M-SC} . However, this might be not the only source of the persistence of a metallic state to lower temperature in the PBE than in the rVV10 model.

On the other hand, in the case of supercooled liquid $\text{Ge}_{15}\text{Sb}_{85}$ the M-SC transition has been associated with the disappearance of a Peierls distortion which amounts to deform an octahedral environment with six bonds into a pyramidal-like with three shorter bonds and three longer ones [24]. This feature has been highlighted by plotting the angular-limited bond correlation (ALTBC) function which measures the probability of finding a bond with length r_1 mostly aligned (within

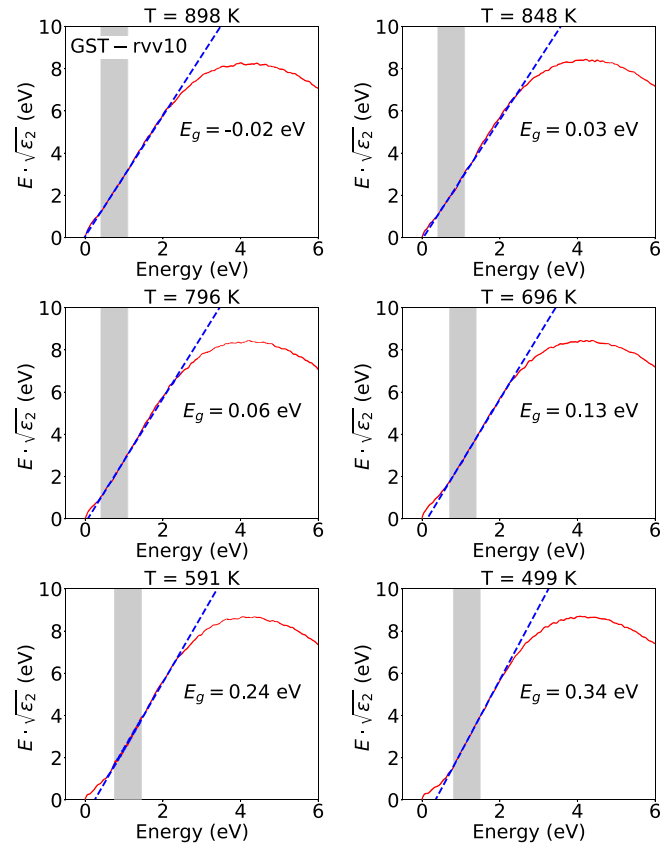


FIG. 4. Tauc plot of liquid and supercooled liquid GST at different temperatures obtained from rVV10 trajectories. The function $\epsilon_2(E)$ is averaged over the same different configurations used for the DOS in Fig. 3. The dielectric function involves only energy differences and thus it does not depend on the choice of the alignment of the DOS in Fig. 3. The shaded area is used for the linear fitting. The resulting Tauc gap is given in each panel and is reported as a function of temperature in Fig. 2. The HSE06 functional was used to compute KS energies.

a threshold angle of 25°) with a second bond of length r_2 formed with the same central atom. The same analysis was also applied to $\text{Ge}_2\text{Sb}_2\text{Te}_5$ and GeTe above and just below T_m in Refs. [8,9] and in earlier work on liquid GeTe [56]. An enhancement of the Peierls distortion was correlated with the

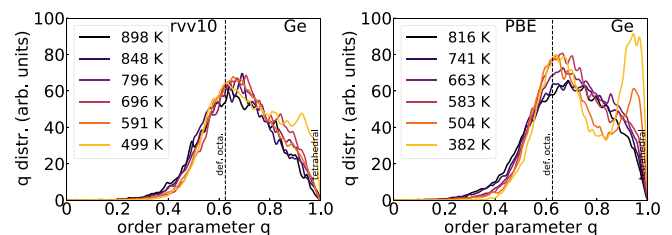


FIG. 5. Distribution of the local order parameter q for four-fold coordinated Ge atoms in liquid $\text{Ge}_2\text{Sb}_2\text{Te}_5$ at different temperatures for (left panel) the rVV10 functional and (right panel) the PBE functional. The coordination number is obtained by integrating the partial pair correlation functions of Fig. 6 up to a cutoff of 3.0, 3.0, 3.2 Å for Ge-Ge; Ge-Sb and Ge-Te pairs.

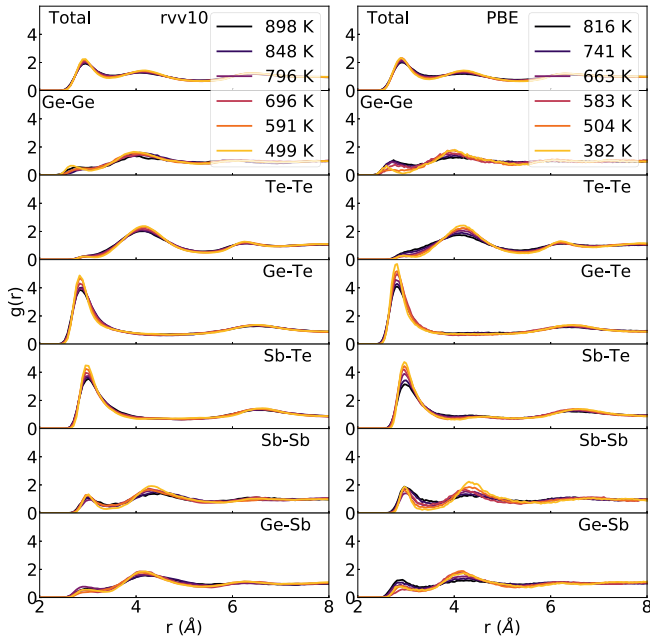


FIG. 6. Total and partial pair correlation functions of GST at different temperatures obtained from simulations with (left panel) the rVV10 functional and (right panel) the PBE functional.

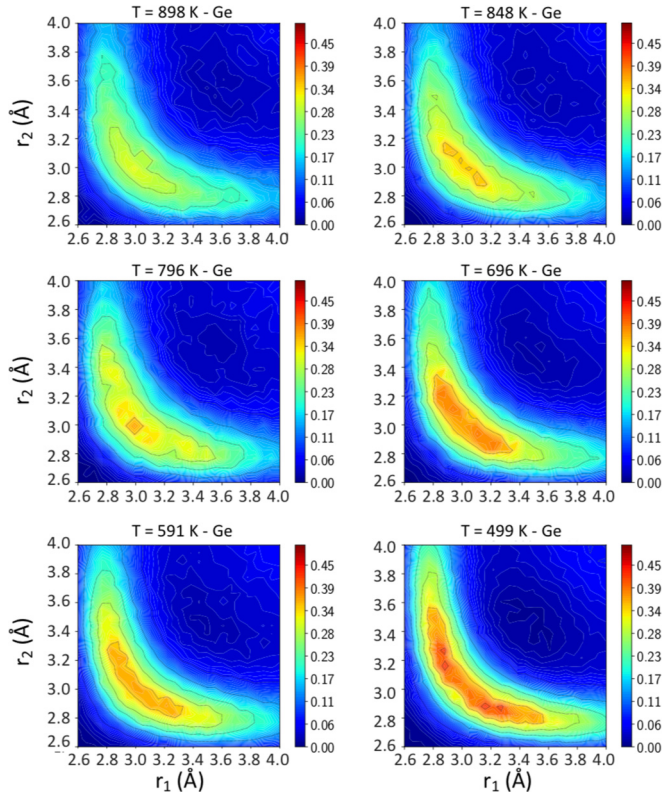


FIG. 7. ALTBC function for $\text{Ge}_2\text{Sb}_2\text{Te}_5$ for Ge atoms for the rVV10 simulations at different temperatures. Radial distances r_1 and r_2 are in Å. The corresponding functions for Sb and Te atoms are reported in Figs. S8 and S9 in the SM [48].

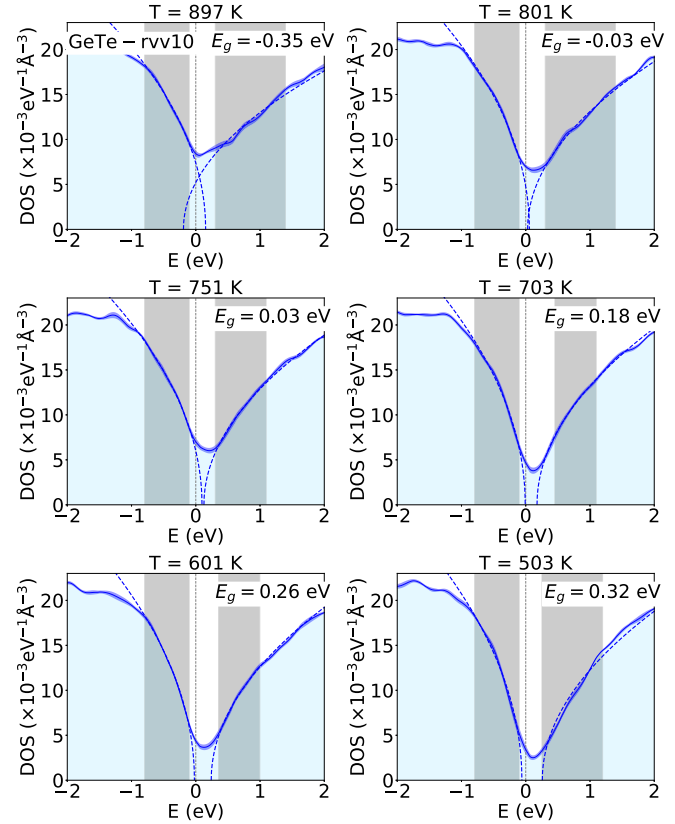


FIG. 8. Electronic density of states (DOS) around the Fermi level of the supercooled liquid GeTe models generated with the rVV10 functional at different temperatures. The DOS are obtained from Kohn-Sham energies computed with the HSE06 functional and broadened with Gaussian functions 27 meV wide. The DOS is averaged over nine configurations at each temperature, the DOS of the different configurations are aligned at the highest occupied state. Standard deviations are depicted by the blue shaded area around the solid lines. Different alignments of the DOS were also checked (see Sec. II). The zero of energy is the Fermi level with the average DOS at each temperature and the constraint on the total number of electrons. The fitting of the conduction and valence band edges with the square-root function $A_c\sqrt{E - E_c}$ and $A_v\sqrt{E_v - E}$ in the gray shaded regions are also shown (dashed lines). The fitting parameters A_v , E_v , A_c , and E_c are given in Table SII in SM [48]. The resulting band gap $E_g = E_c - E_v$ is given in each panel.

deepening of the pseudogap at E_F although the analysis was restricted to temperatures where the DOS at the Fermi level was still relatively high [8,9].

We here extend the same analysis at lower temperatures by reporting the ALTBC function for Ge atoms at different temperatures for the rVV10 functional in Fig. 7. The same plot for the Sb and Te atoms and for all atoms with the PBE functional is shown in Fig. S8–S12 in the SM [48].

At low temperatures a Peierls distortion is clearly visible with a maximum of the ALTBC function at the r_1 – r_2 distances of about 2.8–3.3 Å for rVV10 and 2.8–3.0 Å for PBE. The Peierls distortion fades away continuously by increasing temperature. We notice that the Peierls distortion around Ge atoms vanishes at a lower temperature in PBE than in rVV10 simulations (see Fig. 7 and Fig. S10 in the SM [48]) which

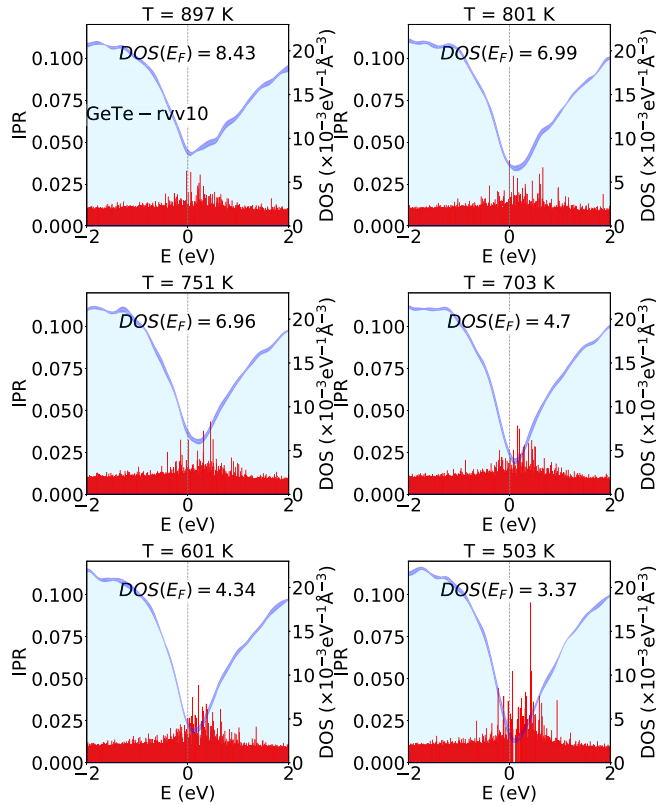


FIG. 9. Electronic density of states (DOS) around the Fermi level of the supercooled liquid GeTe models generated with the rVV10 functional at different temperatures as reported in Fig. 8 with the inverse participation ratio (IPR) superimposed to highlight the rising of localized states in the pseudogap as temperature is lowered. The IPR refers to the same nine configurations used to compute the DOS. The value of the DOS at the Fermi level is given in each panel.

correlates well with a lower T_{M-SC} for the PBE functional inferred from the analysis of the DOS.

The temperature at which the Peierls distortion fades away is higher than the temperature at which the tetrahedra start to appear, although it is still lower than the estimated T_{M-SC} . In the case of $\text{Ge}_{15}\text{Sb}_{85}$ [24], the Peierls distortion is proposed to be responsible of a liquid-liquid phase transition which was also correlated with the M-SC transition. It has been proposed in literature [57] that either a first or a higher order liquid-liquid transition might also occur in other phase change alloys including GeSb_2Te_4 which is structurally very similar to GeTe and $\text{Ge}_2\text{Sb}_2\text{Te}_5$. Our results reveal a correlation between the Peierls distortion and the SC-M transition which, however, better supports a continuous structural change with temperature than a first order phase transition.

Note that the ALTBC of Te (Fig. S9 in SM [48]) shows a persistence of a double peak feature at all temperatures investigated here. The same feature is present in the total (not atom resolved) ALTBC in Ref. [8] above the melting temperature. The longer bond (larger r_i in the two maxima) of the ALTBC of Te atoms is, however, very long, actually about 3.7–3.8 Å which is possibly too much to be associated to a real bond according to the analysis of the bond strength reported in Ref. [58] for GST from the calculation of the

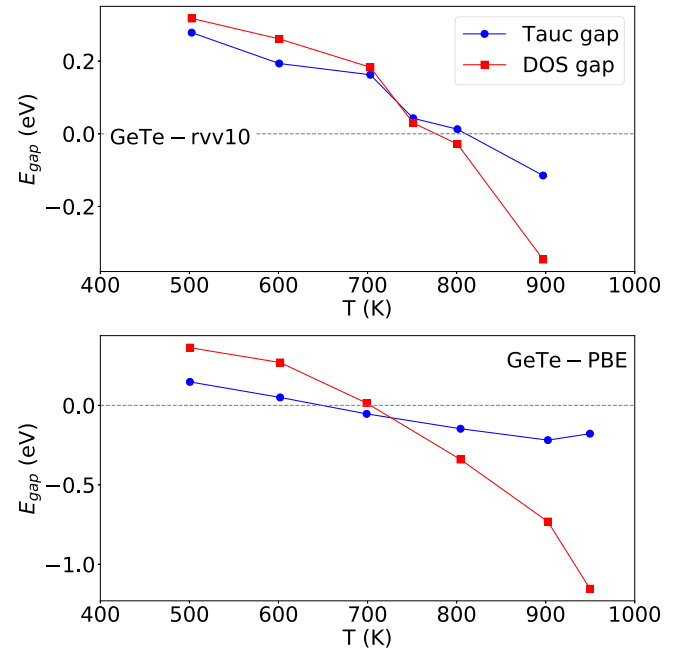


FIG. 10. (Upper panel) Energy gap as a function of temperature in the rVV10 simulations of GeTe given by the Tauc optical gap (blue circles) computed from the plots in Fig. 11 or from the fitting of the electronic DOS close to E_F (red squares) shown in Fig. 8 (see text). (Lower panel) The same of the upper panel for PBE simulations of GeTe. The lines are just a guide for the eye.

Wannier functions and the Electron Localization Function. The disappearance of the double peak feature around Te atoms would occur at much higher temperatures above T_m and it cannot be associated with the opening of a mobility gap in the supercooled liquid phase although it was correlated with other features in the liquid phase such as the negative thermal expansion in Ge-poor GeTe_x alloys [59].

B. GeTe

The DOS close to the Fermi level of supercooled liquid GeTe are reported in Fig. 8 from rVV10 simulations at six different temperatures in the range 500–900 K. As for GST, the DOS close to the pseudogap below and above E_F are fitted by functions of the type $A_v\sqrt{E_v - E}$ and $A_c\sqrt{E - E_c}$ in Fig. 8, where A_v , E_v , A_c , and E_c are fitting parameters given in Table SII in SM [48]. The IPR superimposed to the DOS is shown instead in Fig. 9. The DOS and the IPR over a wider energy range are reported in Fig. S13 and S14 in SM [48] for the rVV10 and PBE functionals.

At the highest temperatures the system is metallic with a high DOS at E_F in agreement with previous DFT calculations [9] using a different vdW functional (DFT-D2) [53]. As occurs in GST, the pseudogap at E_F becomes deeper by decreasing temperature until a gap opens up. The gap $E_g = E_c - E_v$ extracted from the DOS is compared in Fig. 10 with the Tauc gap obtained for rVV10 and PBE functionals. The Tauc plots for rVV10 functional are shown Fig. 11. The DOS and IPR close to E_F and Tauc plots corresponding to the PBE simulations are shown in Figs. S15–S17 in the SM [48].

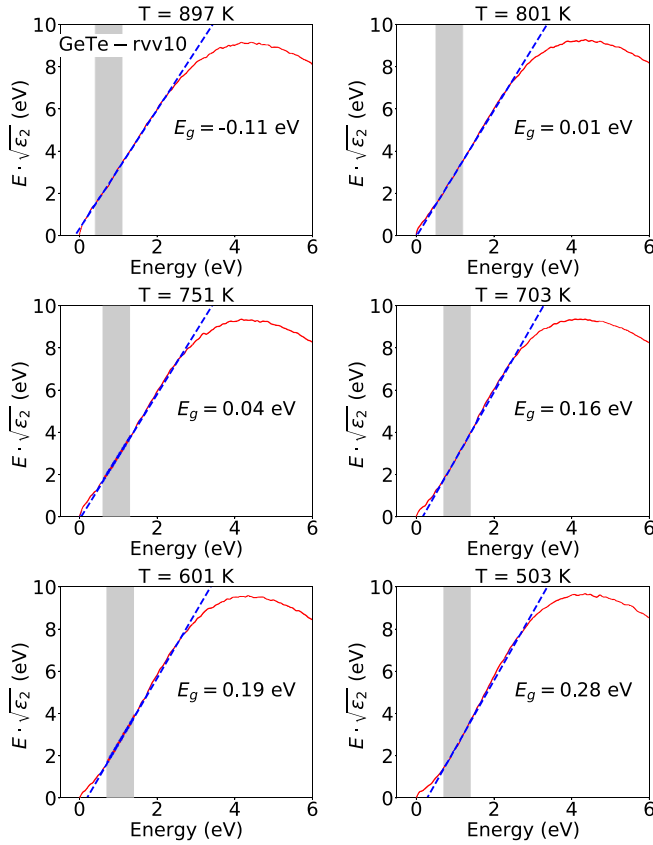


FIG. 11. Tauc plot of liquid and supercooled liquid GeTe at different temperatures obtained from rVV10 trajectories. The function $\varepsilon_2(\omega)$ is averaged over the same different configurations used for the DOS in Fig. 9. The shaded area is used for the linear fitting. The resulting Tauc gap is given in each panel and reported as a function of temperature in Fig. 10. The HSE06 functional was used to compute KS states.

The Tauc gap and the gap extracted from the DOS both vanish at about 800 K with the rVV10 functional. On the contrary, a sizable difference is observed in the band gap closure from the two methods with the PBE functional which yields T_{M-SC} in the range 650–700 K. This is due to some uncertainties in the fitting of the conduction band with a square root of the energy for the PBE-DOS (see Fig. 8). Still, T_{M-SC} is fairly lower for the PBE simulations as occurs for GST. In this respect the same argument proposed for GST holds here for GeTe, i.e., a higher DOS at E_F at high temperatures might be due to a higher content of Ge-Ge bonds in the PBE simulations as shown by the partial pair correlation functions reported in Fig. 12. Similarly to GST, there is no correlation between the disappearance of tetrahedra with temperature and the closure of the mobility gap. The distribution of the q order parameter for GeTe reported in Fig. 13 shows the appearance of a peak due to tetrahedra at temperatures much lower than T_{M-SC} estimated from the closure of the band gap. The bond angle distribution functions and the distribution of coordination numbers for GeTe with the rVV10 and PBE functionals are shown in Figs. S18 and S19 in the SM [48].

The ALTBC function for Ge atoms in GeTe with the rVV10 functional is reported in Fig. 14 for different temper-

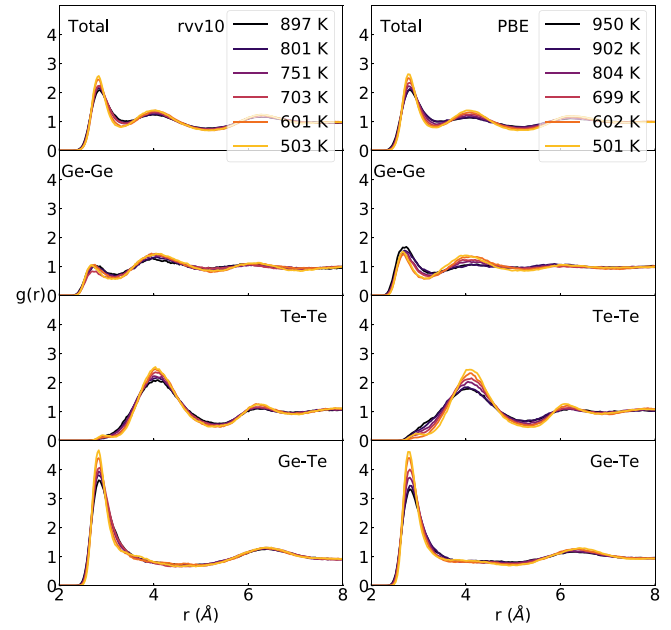


FIG. 12. Total and partial pair correlation functions of GeTe at different temperatures obtained from simulations with (left panel) the rVV10 functional and (right panel) the PBE functional.

atures. The ALTBC functions for Te atoms with the rVV10 functional and for all atoms with the PBE functional are shown in Figs. S20–S22 in the SM [48]. Similar to GST, a Peierls distortion around the Ge atoms is visible at low temperatures at the r_1 – r_2 distances of about 2.8–3.4 Å for rVV10 and 2.85–3.0 Å for PBE.

Concerning the ALTBC for Te atoms (Fig. S20 in SM [48]) the same remarks raised in the discussion for GST holds here for GeTe.

The Peierls distortion is blurred at a lower temperature in PBE than in rVV10 simulations which correlates with a lower T_{M-SC} estimated from the PBE band gap. Similarly to GST, the temperature at which the Peierls distortion vanishes is higher than the temperature at which the tetrahedra appear, although it is still sizably lower than T_{M-SC} . Therefore, albeit a

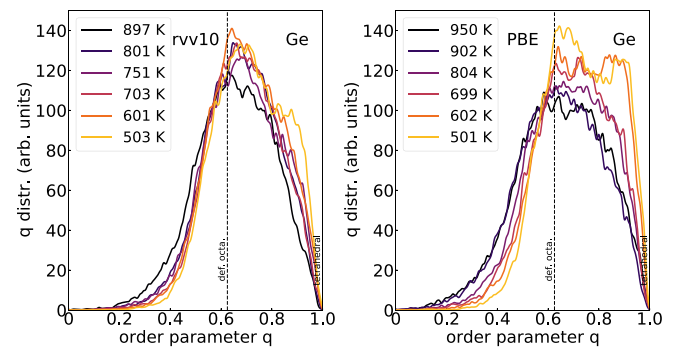


FIG. 13. Distribution of the local order parameter q for four-fold coordinated Ge atoms in liquid GeTe at different temperatures for (left panel) the rVV10 functional and (right panel) the PBE functional. The coordination number is obtained by integrating the partial pair correlation functions of Fig. 12 up to a cutoff of 3.0 and 3.22 Å for Ge-Ge and Ge-Te pairs.

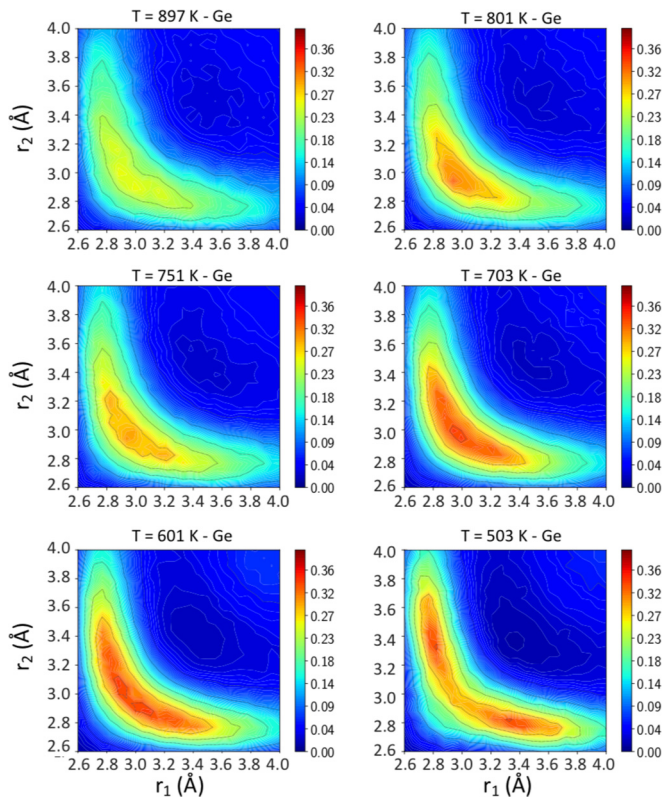


FIG. 14. ALTBC function for GeTe for Ge atoms in the rVV10 simulations at different temperatures. Radial distances r_1 and r_2 are in Å. The corresponding functions for Te atoms are reported in Fig. S20 in the SM [48].

correlation between the Peierls distortion and the M-SC transition is indeed possible, also for GeTe the structural transformation associated with the M-SC transition seems continuous and not a first order phase change.

We remark that the value $T_{M-SC} = 800$ K inferred from rVV10 simulation is actually equal to the estimate given in Ref. [21] where it is assumed that the T_{M-SC} corresponds to a maximum in the specific heat. The temperature for the maximum in the specific heat for GeTe was obtained in turn by extrapolating to the GeTe composition the corresponding values known experimentally for other GeTe_x alloys richer in tellurium [21].

IV. CONCLUSIONS

We have investigated the opening of the gap in the electronic density of states of the supercooled liquid phase of $\text{Ge}_2\text{Sb}_2\text{Te}_5$ and GeTe by DFT simulations. We have tentatively identified the presence of a mobility gap in two manners. On the one hand, we fitted the edge of the valence

and conduction bands with a square root function of the energy to assign the band edges and we then verified whether the states in the gap are localized by looking at the inverse participation ratio. On the other hand, we computed the Tauc plot from the imaginary part of the dielectric function which is another measure of the gap that still assumes a square root shape of valence and conduction bands close to the edges. The two methods give fairly similar results for the temperature at which the gap opens up in the supercooled liquid phase which we identify with the temperature of the metal-semiconductor transition T_{M-SC} . However, we observed a sizable difference in the estimated T_{M-SC} with the PBE and rVV10 approximations for the exchange and correlation functionals, the latter including van der Waals interactions. For GST, the estimated T_{M-SC} is about 850 K (700 K) for the rVV10 (PBE) functional. In the case of GeTe, the estimated T_{M-SC} (rVV10) is much closer to T_m (858–877 K [16,40]) than to the glass transition temperature which is $T_g = 373$ K [60] or $T_g = 473$ K [61] as obtained from differential scanning calorimetry. For GeTe the estimated T_{M-SC} is deeper in the supercooled liquid. However, if we consider the rVV10 functional more reliable than the PBE functional given the previous evidence on the importance of the vdW interactions in these systems, then it is still true that T_{M-SC} is closer to the melting temperature ($T_m = 998$ K [39]) than to the glass transition temperature ($T_g = 412$ K [20]) for GeTe as well.

The analysis of the structural properties as a function of temperature seems to exclude a correlation between the appearance of tetrahedra at high supercooling and the opening of a mobility gap which occurs at a much higher temperature closer to T_m . A better correlation is found between the M-SC transition and the Peierls distortion which appears at higher temperature, although still sizably lower than the estimated T_{M-SC} . Therefore, our results support more the presence of a continuous structural change responsible for the M-SC than a first order liquid-liquid phase transition. As a final remark we mention that our estimated T_{M-SC} is actually close to the temperature at which an anomaly in the viscosity is observed in previous DFT simulations of $\text{Ge}_2\text{Sb}_2\text{Te}_5$ [62].

ACKNOWLEDGMENTS

We thank L. Hartmann for her contribution in the preliminary part of the project. We thankfully acknowledge the computational resources provided by the ISCRA program at Cineca (Casalecchio di Reno, Italy). This work was partly funded by the European Union's Horizon 2020 research and innovation programme under Grant Agreement No. 824957 (BeforeHand: Boosting Performance of Phase Change Devices by Hetero- and Nanostructure Material Design).

- [1] S. W. Fong, C. M. Neumann, and H.-S. P. Wong, *IEEE Trans. Electron. Devices* **64**, 4374 (2017).
- [2] M. Wuttig and N. Yamada, *Nat. Mater.* **6**, 824 (2007).
- [3] A. Pirovano, A. L. Lacaita, A. Benvenuti, F. Pellizzer, and R. Bez, *IEEE Trans. Electron. Devices* **51**, 452 (2004).
- [4] P. Noé, C. Vallée, F. Hippert, F. Fillot, and J.-Y. Raty, *Semicond. Sci. Technol.* **33**, 013002 (2018).

- [5] G. E. Ghezzi, J.-Y. Raty, S. Maitrejean, A. Roule, E. Elkaim, and F. Hippert, *Appl. Phys. Lett.* **99**, 151906 (2011).
- [6] P. Zuliani, E. Palumbo, M. Borghi, G. Dalla Libera, and R. Annunziata, *Solid-State Electron.* **111**, 27 (2015).
- [7] D. Lencer, M. Salinga, and M. Wuttig, *Adv. Mater.* **23**, 2030 (2011).

- [8] M. Schumacher, H. Weber, P. J v ari, Y. Tsuchiya, T. G. A. Youngs, I. Kaban, and R. Mazzarello, *Sci. Rep.* **6**, 27434 (2016).
- [9] H. Weber, M. Schumacher, P. J v ari, Y. Tsuchiya, W. Skrotzki, R. Mazzarello, and I. Kaban, *Phys. Rev. B* **96**, 054204 (2017).
- [10] J. Akola and R. O. Jones, *J. Phys.: Condens. Matter* **20**, 465103 (2008).
- [11] J.-Y. Raty, V. Godlevsky, Ph. Ghosez, C. Bichara, J. P. Gaspard, and J. R. Chelikowsky, *Phys. Rev. Lett.* **85**, 1950 (2000); J.-P. Gaspard, A. Pellegatti, F. Marinelli, and C. Bichara, *Philos. Mag. B* **77**, 727 (1998).
- [12] S. Caravati, D. Colleoni, R. Mazzarello, T. Kuhne, M. Krack, M. Bernasconi, and M. Parrinello, *J. Phys.: Condens. Matter* **23**, 265801 (2011).
- [13] D. Dragoni and M. Bernasconi, *J. Chem. Phys.* **151**, 134503 (2019).
- [14] R. Endo, S. Maeda, Y. Jinnai, R. Lan, M. Kuwahara, Y. Kobayashi, and M. Susa, *Jpn. J. Appl. Phys.* **49**, 065802 (2010).
- [15] V. A. Alekseev, A. A. Andreev, and M. V. Sadowskii, *Sov. Phys. Usp.* **23**, 551 (1980).
- [16] K. Cil, F. Dirisaglik, L. Adnane, M. Wennberg, A. King, A. Faraclas, M. B. Akbulut, Y. Zhu, C. Lam, A. Gokirmak, and H. Silva, *IEEE Trans. Electron. Devices* **60**, 433 (2013).
- [17] S. Wei, P. Lucas, and C. A. Angell, *MRS Bull.* **44**, 691 (2019).
- [18] J. Orava, A. L. Greer, B. Gholipour, D. W. Hewak, and C. E. Smith, *Nat. Mater.* **11**, 279 (2012).
- [19] G. C. Sosso, J. Behler, and M. Bernasconi, *Phys. Status Solidi B* **249**, 1880 (2012).
- [20] Y. Chen, G. Wang, L. Song, X. Shen, J. Wang, J. Huo, R. Wang, T. Xu, S. Dai, and Q. Nie, *Cryst. Growth Des.* **17**, 3687 (2017).
- [21] S. Wei, G. J. Coleman, P. Lucas, and C. A. Angell, *Phys. Rev. Appl.* **7**, 034035 (2017).
- [22] S. Wei, P. Lucas, and C. A. Angell, *J. Appl. Phys.* **118**, 034903 (2015).
- [23] T. Wang, O. Gulbiten, R. Wang, Z. Yang, A. Smith, B. Luther-Davies, and P. Lucas, *J. Phys. Chem. B* **118**, 1436 (2014).
- [24] P. Zalden *et al.*, *Science* **364**, 1062 (2019).
- [25] J. VandeVondele, M. Krack, F. Mohamed, M. Parrinello, T. Chassaing, and J. Hutter, *Comput. Phys. Commun.* **167**, 103 (2005).
- [26] M. Krack and M. Parrinello, *High Performance Computing in Chemistry*, Vol. 25, edited by J. Grotendorst (John von Neumann Institute for Computing (NIC), J lich, 2004), pp. 29–51; www.cp2k.org.
- [27] S. Goedecker, M. Teter, and J. Hutter, *Phys. Rev. B* **54**, 1703 (1996); M. Krack, *Theor. Chem. Acc.* **114**, 145 (2005).
- [28] S. Caravati, M. Bernasconi, T. D. K hne, M. Krack, and M. Parrinello, *J. Phys.: Condens. Matter* **21**, 255501 (2009); **21**, 499803(E) (2009); **22**, 399801(E) (2010).
- [29] R. Mazzarello, S. Caravati, S. Angioletti-Uberti, M. Bernasconi, and M. Parrinello, *Phys. Rev. Lett.* **104**, 085503 (2010).
- [30] S. Caravati, M. Bernasconi, T. D. K hne, M. Krack, and M. Parrinello, *Appl. Phys. Lett.* **91**, 171906 (2007).
- [31] J. H. Los, T. D. K hne, S. Gabardi, and M. Bernasconi, *Phys. Rev. B* **88**, 174203 (2013).
- [32] E. Spreafico, S. Caravati, and M. Bernasconi, *Phys. Rev. B* **83**, 144205 (2011).
- [33] A. Bouzid, S. Gabardi, C. Massobrio, M. Boero, and M. Bernasconi, *Phys. Rev. B* **91**, 184201 (2015).
- [34] O. A. Vydrov and T. van Voorhis, *J. Chem. Phys.* **133**, 244103 (2010).
- [35] R. Sabatini, T. Gorni, and S. de Gironcoli, *Phys. Rev. B* **87**, 041108(R) (2013).
- [36] J. P. Perdew, K. Burke, and M. Ernzerhof, *Phys. Rev. Lett.* **77**, 3865 (1996).
- [37] T. D. K hne, M. Krack, F. R. Mohamed, and M. Parrinello, *Phys. Rev. Lett.* **98**, 066401 (2007).
- [38] T. D. K hne, M. Krack, and M. Parrinello, *J. Chem. Theory Comput.* **5**, 235 (2009).
- [39] W. Klemm and G. Frischmuth, *Z. Anorg. Chem.* **218**, 249 (1934).
- [40] A. Sebastian, M. Le Gallo, and D. Krebs, *Nat. Commun.* **5**, 4314 (2014).
- [41] G. C. Sosso, G. Miceli, S. Caravati, J. Behler, and M. Bernasconi, *Phys. Rev. B* **85**, 174103 (2012).
- [42] Y. Li and R. Mazzarello, *Adv. Mater.* **24**, 1429 (2012).
- [43] F. C. Mocanu, K. Konstantinou, and S. R. Elliott, *J. Phys. D: Appl. Phys.* **53**, 244002 (2020).
- [44] S. Gabardi, G. C. Sosso, J. Behler, and M. Bernasconi, *Faraday Discuss.* **213**, 287 (2019).
- [45] J. Kalikka, J. Akola, and R. O. Jones, *Phys. Rev. B* **94**, 134105 (2016).
- [46] G. C. Sosso, G. Miceli, S. Caravati, F. Giberti, J. Behler, and M. Bernasconi, *J. Phys. Chem. Lett.* **4**, 4241 (2013).
- [47] A. V. Krukau, O. A. Vydrov, A. F. Izmaylov, and G. E. Scuseria, *J. Chem. Phys.* **125**, 224106 (2006).
- [48] See Supplemental Material at <http://link.aps.org/supplemental/10.1103/PhysRevMaterials.5.045004> for additional information on the structural and electronic properties of the supercooled liquid phase of GeTe and Ge₂Sb₂Te₅.
- [49] W. Welnic, M. Wuttig, S. Botti, and L. Reining, *C. R. Phys.* **10**, 514 (2009).
- [50] S. Caravati, M. Bernasconi, and M. Parrinello, *J. Phys.: Condens. Matter* **22**, 315801 (2010).
- [51] J. Im, E. Cho, D. Kim, H. Horii, J. Ihm, and S. Han, *Phys. Rev. B* **81**, 245211 (2010).
- [52] F. Zipoli, D. Krebs, and A. Curioni, *Phys. Rev. B* **93**, 115201 (2016).
- [53] K. Lee, E. D. Murray, L. Kong, B. I. Lundqvist, and D. C. Langreth, *Phys. Rev. B* **82**, 081101(R) (2010).
- [54] J. R. Errington and P. G. Debenedetti, *Nature* **409**, 318 (2001).
- [55] S. Gabardi, S. Caravati, G. C. Sosso, J. Behler, and M. Bernasconi, *Phys. Rev. B* **92**, 054201 (2015).
- [56] J. Y. Raty, V. V. Godlevsky, J. P. Gaspard, C. Bichara, M. Bionducci, R. Bellissent, R. Ce olin, J. R. Chelikowsky, and Ph. Ghosez, *Phys. Rev. B* **65**, 115205 (2002).
- [57] P. Lucas, S. Wei, and C. A. Angell, *Int. J. Appl. Glass. Sci.* **11**, 236 (2020).
- [58] T. H. Lee and S. R. Elliott, *Adv. Mater.* **29**, 1700814 (2017).
- [59] J.-P. Gaspard, *C. R. Phys.* **17**, 389 (2016).
- [60] E. Morales-S nchez, E. F. Prokhorov, A. Mendoza-Galv n, and J. Gonz lez-Hern ndez, *J. Appl. Phys.* **91**, 697 (2002).
- [61] J. Pries, S. Wei, M. Wuttig, and P. Lucas, *Adv. Mater.* **31**, 1900784 (2019).
- [62] H. Flores-Ruiz and M. Micoulaut, *J. Chem. Phys.* **148**, 034502 (2018).